Journal of Solid State Chemistry 182 (2009) 3342–3352

Contents lists available at ScienceDirect

Journal of Solid State Chemistry

journal homepage: www.elsevier.com/locate/jssc

Structural and spectroscopic characterization of $Mo_{1-x}W_xO_{3-\delta}$ mixed oxides

S. Morandi [a], M.C. Paganini [a], E. Giamello [a], M. Bini [b], D. Capsoni [b], V. Massarotti [b], G. Ghiotti [a,*]

[a] Department of Inorganic, Physical and Materials Chemistry and NIS Center of Excellence, University of Torino, Via P. Giuria 7-9, 10125 Torino, Italy
[b] Department of Physical Chemistry "M. Rolla" and IENI-CNR, University of Pavia, Viale Taramelli 16, 27100 Pavia, Italy

ARTICLE INFO

Article history:
Received 5 March 2009
Received in revised form
10 September 2009
Accepted 20 September 2009
Available online 30 September 2009

Keywords:
Semiconducting oxides
FT-IR
UV–vis–NIR
EPR
XRD
Rietveld refinement

ABSTRACT

$Mo_{1-x}W_xO_3$ oxides with different cationic fraction (x=0.2, 0.5 and 0.8) and, for comparison purposes, pure MoO_3 and WO_3 were prepared. Along with textural and structural characterizations, absorbance FT-IR, diffuse reflectance UV–vis–NIR and EPR spectroscopies were employed to study the changes in the electronic properties of these materials passing from $Mo_{1-x}W_xO_3$ in oxidizing atmosphere to $Mo_{1-x}W_xO_{3-\delta}$ in reducing conditions. XRD analysis showed that the Mo–W mixed oxides are constituted by two or three crystalline phases, whose abundance and composition are well characterized by structural refinement with the Rietveld method. Only the sample with the highest Mo content (x=0.2) shows a predominant mixed phase and also a superior ability to lose oxygen with respect to the other mixed oxides. The oxygen loss in the reduced oxides induces the formation of defects with electronic levels in the band gap of the material, in particular, electrons trapped in oxygen vacancies and/or at cationic sites (polarons). While the nature of defect sites induced in the mixed and in the pure oxides is similar, the photo-ionization energies, the ratio between surface and bulk defects and the stability of the defects in oxygen at increasing temperature are peculiar of each mixed oxide.

1. Introduction

Due to their interesting optical and electronic properties MoO_3 and WO_3 find application in a variety of solid-state electronic devices. Tungsten oxide is by far the most extensively studied in the field of electrochromic materials, which are currently of interest for displays, rearview mirrors and smart windows [1–3]. Furthermore, molybdenum and tungsten oxide based materials are highly important in selective oxidation catalysis [4–6] and tungsten oxide based materials are studied as photo-catalysts for organic compound decomposition [7].

Perfectly stoichiometric MoO_3 and WO_3 are insulators. However, it is well known that these oxides are able to lose oxygen from the lattice already at low temperature in vacuum or at very low oxygen partial pressure, leaving excess electrons in the solid and giving rise to electrical conductivity, primarily due to thermal activated hopping of polarons [8–12]. At high temperatures the oxygen loss under vacuum can be so drastic that the well-known crystallographic shear defect process takes place [13,14].

The semiconducting properties make them also attractive for applications in gas-sensing field. In particular, WO_3 has shown good NO_2 sensing capability [15,16] and MoO_3 good sensitivity to CO and NO_2 [17,18]. Sometimes, metal oxide combinations allow obtaining desired properties and better performances. As a matter of fact, recent studies focused on MoO_3–WO_3 mixed oxides report on their promising gas-sensing potential [19–22]. In the past MoO_3, WO_3 and MoO_3–WO_3 mixed oxides were deeply studied mainly by optical spectroscopy and structural analysis [9,14,23–31]. The recently obtained interesting results about the structural, spectroscopic and electrical characterization of these systems prepared as thin films deposited by radio frequency magnetron sputtering on alumina and silicon substrates [32,33] stimulated and induced us to continue with the characterization of this type of materials. The major novelty of the present paper is the employ of FT-IR spectroscopy (rarely used) with the aim to individuate the presence of electronic transitions falling in the medium IR region.

Actually, the FT-IR spectroscopy combined with EPR technique and UV–vis–NIR spectroscopy, allowed new interesting observations on the investigated systems with respect to what known in literature. We synthesized powders of mixed Mo–W oxides $Mo_{1-x}W_xO_3$ with x values 0.2, 0.5 and 0.8 and, for comparison purposes, also pure MoO_3 and WO_3. Textural and structural characterizations were performed by volumetric measurements and X-ray powder diffraction analysis (XRD), respectively. In particular the abundance and composition of each phase present in the system are evaluated by the Rietveld method. Spectroscopic characterization of electronic changes induced by thermal treatments in vacuum and in dry oxygen was carried out by absorbance FT-IR, diffuse reflectance UV–vis–NIR and EPR spectroscopies.

* Corresponding author. Fax: +39 0116707855.
E-mail address: giovanna.ghiotti@unito.it (G. Ghiotti).

0022-4596/$ - see front matter © 2009 Elsevier Inc. All rights reserved.
doi:10.1016/j.jssc.2009.09.025

2. Experimental

2.1. Sample preparations

Molybdenum and tungsten oxides were prepared starting from 100 ml of $(NH_4)_6Mo_7O_{24}\cdot 4H_2O$ and $(NH_4)_{10}W_{12}O_{41}\cdot 7H_2O$ aqueous solutions 0.2 and 0.03 M, respectively (the solubility of tungsten salt is drastically lower than that of the correspondent molybdenum salt), maintained at 353 K. The hydrated oxides were precipitated by adding HNO_3 3 M. The white and light yellow precipitates obtained were washed with distilled water, dried at 333 K and then calcined for 12 h at increasing temperature up to 723 K in oxygen flow, obtaining powders of MoO_3 (gray) and WO_3 (light green).

The powders of the mixed molybdenum tungsten oxides $Mo_{1-x}W_xO_3$ were prepared with nominal cationic fraction values, x=0.2, 0.5 and 0.8: in the following these samples will be named MoW02, MoW05 and MoW08, respectively. The stoichiometric amounts of $(NH_4)_6Mo_7O_{24}\cdot 4H_2O$ and $(NH_4)_{10}W_{12}O_{41}\cdot 7H_2O$ were dissolved in water at 353 K to obtain solutions with total concentration equal to 0.12 M, then the corresponding mixed hydrated oxides were precipitated by HNO_3 3 M. The precipitates were washed with distilled water, dried at 333 K and calcined for 12 h at increasing temperature up to 723 K in oxygen flow, obtaining light green powders. The elemental analysis confirmed that the nominal cationic fractions were maintained.

The final calcination temperature of 723 K was chosen as a trade off between the need for the same annealing temperature for these powders and good thermal stability: (i) MoO_3, when annealed between 673 and 773 K, shows orthorhombic structure and it starts to sublimate at temperature above approximately 973 K; (ii) WO_3 well crystallizes in the monoclinic form at 673 K and is stable at temperature even higher than 973 K.

2.2. Characterization techniques

Specific surface areas and pore size distributions were determined by volumetric measurements with N_2 adsorption at 77 K with a Micromeritics ASAP 2100 apparatus on the powders outgassed at 523–573 K and 10^{-3} mbar.

X-ray diffraction (XRD) measurements were performed in air at room temperature (RT) on a Bruker D5005 diffractometer with Cu$K\alpha$ radiation ($K\alpha1$ = 1.54056 Å, $K\alpha2$ = 1.54439 Å, 40 kW, 30 mA), Ni filter and a position sensitive detector (PSD). Patterns were collected in the angular range $10^\circ < 2\theta < 70^\circ$ in steps of 0.015° with 0.6 s of counting time. Structural and profile parameters, phase abundance percentages and cation distribution in the solid solutions were obtained by the Rietveld refinement of multiphase systems performed with TOPAS 3.0 program [34]. The structural parameters were optimized starting from database structural data.

For diffuse reflectance UV–vis–NIR and for EPR analyses the powders were placed in quartz home-made cells, for the FT-IR characterization the powders were compressed in self-supporting disks and placed in IR home-made cell. Absorbance IR spectra were run at RT on a Perkin-Elmer System 2000 FT-IR spectrophotometer equipped with a Hg–Cd–Te cryodetector, working in the range of wavenumbers 7800–580 cm^{-1}. Diffuse reflectance UV–vis–NIR spectra were run at RT on a Varian Cary 5 spectrophotometer, working in the range of wavenumbers 53000–4000 cm^{-1}. In the figures we used the Kubelka-Munk function [$f(R_\infty)=(1-R_\infty)^2/2R_\infty$; R_∞ = reflectance of an "infinitely thick" layer] that is comparable to the absorbance of the FT-IR spectra.

Electron paramagnetic resonance (EPR) spectra were recorded at 77 K and in some cases at 4 K on a Bruker EMX instrument working in X-band (9.5 GHz).

For spectroscopic analyses, the samples were first activated at 723 K, i.e. treated in vacuum (20 min) to clean the sample from water, carbonates and other adsorbed species, then in dry oxygen (20 min, $p_{O_2} \approx 40$ mbar) and, eventually, they were cooled down to room temperature and a spectrum was run. Then the samples underwent treatments in vacuum at RT, 473, 573 and 673 K and, subsequently, in dry O_2 (30 mbar) at RT, 473, 573 and 673 K. After treatment at each temperature a spectrum was run at RT in the medium IR (MIR) and UV–vis–NIR region, at 77 K in the case of EPR technique. It is important to point out that the UV–vis–NIR and EPR spectra are reported in the figures without any manipulation. Conversely, where indicated, the FT-IR spectra (spectra in the MIR region) are reported as difference spectra, where the spectrum subtracted is always the one recorded after outgassing and oxidation at 723 K. In other words, the MIR spectrum of the sample after the activation is considered as a background to which all the other MIR spectra are referred. This elaboration is useful only for the spectra in the MIR region, where features due to vibrational modes and to the radiation scattering are present: in this way difference spectra put in evidence only the changes induced by the treatments.

3. Results and discussion

3.1. Textural and structural characterization

MoO_3, WO_3, MoW02, MoW05 and MoW08 powders calcined at 723 K show BET surface areas of 3, 13, 5, 5 and 4 m^2/g, respectively. MoO_3, MoW02 and MoW05 do not present micro- or meso-porosity, while for both WO_3 and MoW08 N_2 adsorption and desorption isotherms show the hysteresis loop typical of meso-porous materials, with pore diameter ranging between 40 and 100 Å. It is usually difficult to obtain these oxides with high surface areas. However, the low specific surface area does not correspond to very large particle sizes because these materials possess high densities. In the case of non-porous materials (MoO_3, MoW02 and MoW05), assuming particles with spherical shapes, the average diameter ranges from some tens to few hundreds of nanometers.

XRD patterns were collected for all the samples after calcination at 723 K in oxygen flow (oxidized samples) and after treatment under vacuum at 673 K (reduced samples), to verify the structural stability under reducing conditions.

Oxidized MoO_3 and WO_3 show diffraction peaks characteristic of the orthorhombic (α-MoO_3) and monoclinic (γ-WO_3) phases, respectively. After treatment under vacuum at 673 K for 2 h, no change is observed in the XRD patterns of MoO_3 and WO_3. However, the changes of the sample color and of the spectroscopic features (see below) suggest the creation of defect sites. As mentioned above, it is well known that, for molybdenum and tungsten oxides, oxygen vacancies can be eliminated by crystallographic shear process. Probably, the amount of defects induced by the heating is not enough to bring large structural changes, which remain under the detection limit of X-ray diffraction. Another hypothesis could be that oxygen is lost only from the surface or sub-surface layers and the bulk is unaffected. We will see that spectroscopic results exclude this last hypothesis.

The XRD patterns of the oxidized and reduced mixed oxides are shown in Fig. 1A. These samples are constituted by two or three crystalline phases that, together with the pertinent JCPDS card number, are reported in Table 1 along with their weight

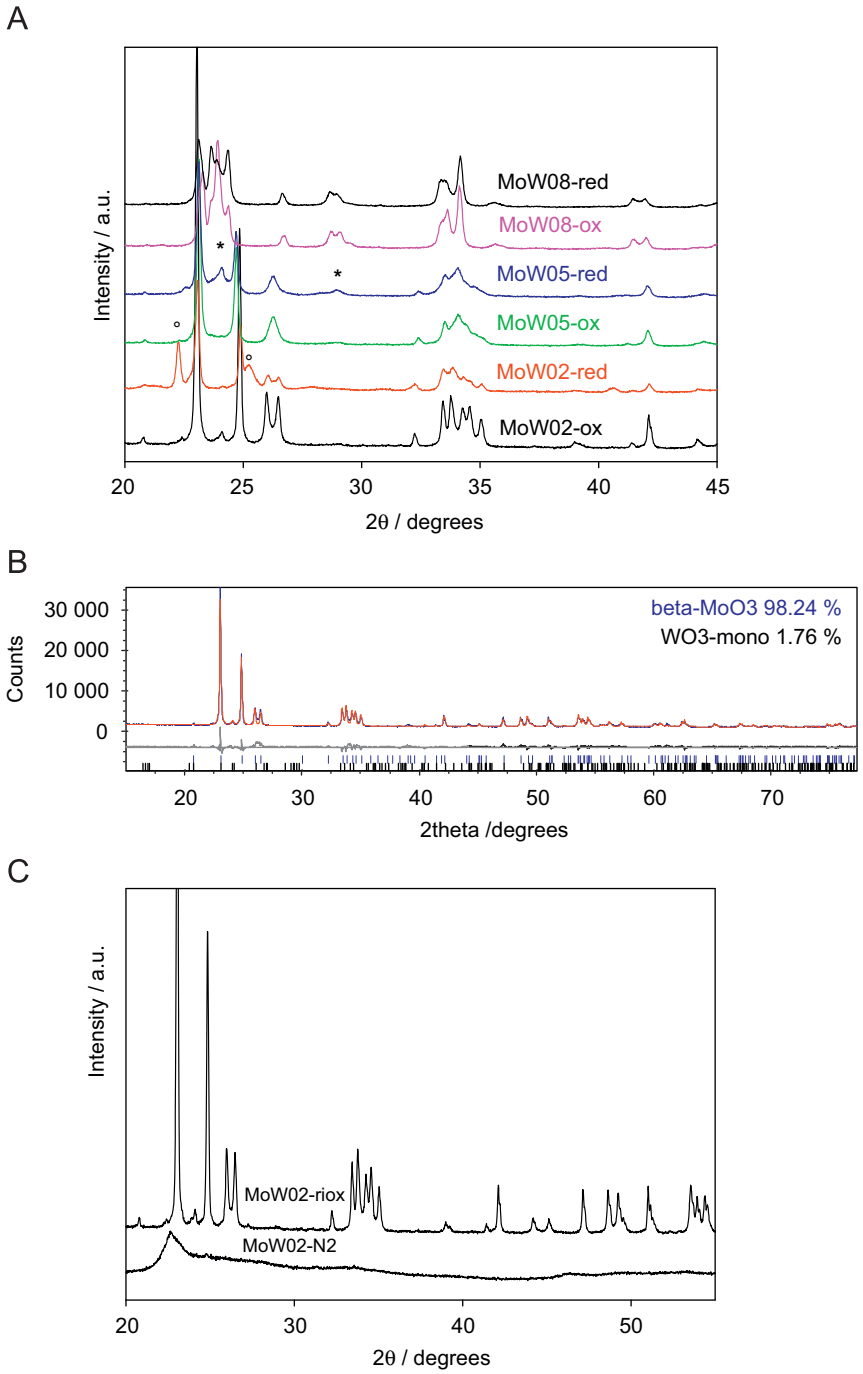

Fig. 1. Section A: XRD patterns of MoW02, MoW05 and MoW08 calcined in oxygen at 723 K (ox) and reduced in vacuum at 673 K (red). The main peaks of γ-WO_3 (*) and of $Mo_{0.85}W_{0.15}O_{2.91}$ sub-stoichiometric (◦) phases are evidenced. Section B: Rietveld refinement of MoW02 oxidized sample: the experimental pattern (blue line) is compared with the calculated one (red line). The difference pattern and the bars indicating the reflection peak positions of the refined structures are also shown in the bottom. Section C: XRD patterns of MoW02 treated in N_2 at 723 K and subsequently oxidized at 723 K (coincident with that of MoW02 directly oxidized).

percentages, obtained by the Rietveld refinement. For the mixed oxide samples in which the β-MoO_3 phase is observed, the capability to partially substitute the W cation on Mo sites was investigated: the W amount on each of the two Mo crystallographic sites of the β-MoO_3 structure was refined under a suitable constraint (each site is completely occupied by the W+Mo amount). The same approach was used to investigate the partial Mo substitution on the two crystallographic sites of W ion in the γ-WO_3 structure. The literature composition for the $Mo_{0.6}W_{0.4}O_3$, $Mo_{0.29}W_{0.71}O_3$ and $Mo_{0.85}W_{0.15}O_{2.91}$ mixed oxides was not refined. The pertinent sample stoichiometry was calculated by taking into account both the stoichiometries and the phase percentages of the components and was reported in Table 1. The Rietveld refinement results are satisfactory and the experimental patterns are well fitted; as an example the Rietveld refinement on the pattern of oxidized MoW02 sample is shown in Fig. 1B. Concerning the oxidized samples, only MoW02 shows a predominant mixed phase with the structure of β-MoO_3 [35] and W occupancy of 0.21(1). The monoclinic WO_3 phase without substitution [36] is present in very low amount (main peaks indicated by * in Fig. 1A). The α-MoO_3 form, obtained for the pure sample, is not stable for $x \geq 0.20$ W substitution, where the

Table 1
Stoichiometry and weight percentages (standard deviations in brackets) of the crystalline phases present in oxidized and reduced Mo–W mixed oxides.

Phases	MoW02		MoW05		MoW08	
	Ox	Red	Ox	Red	Ox	Red
β-MoO_3 (monoclinic) #89-1554	$Mo_{0.79(1)}W_{0.21(1)}O_3$ 98.3(1.0)	$Mo_{0.81(2)}W_{0.19(2)}O_3$ 61.1(1.0)	$Mo_{0.49(4)}W_{0.51(4)}O_3$ 46.6(1.0)	$Mo_{0.67(4)}W_{0.33(4)}O_3$ 29.7(1.0)		
γ-WO_3 (monoclinic) #83-0950	1.7(1.0)	0.9(1.0)		25.4(1.0)	$Mo_{0.14(6)}W_{0.86(6)}O_3$ 33.3(1.0)	$Mo_{0.07(4)}W_{0.93(4)}O_3$ 60.6(1.0)
$Mo_{0.6}W_{0.4}O_3$ #76-1280			49.7(1.0)	44.9(1.0)		
$Mo_{0.29}W_{0.71}O_3$ #76-1279			3.7(1.0)		66.7(1.0)	39.4(1.0)
$Mo_{0.85}W_{0.15}O_{2.91}$ #73-2198		38.0(1.0)				
Global stoichiometry	$Mo_{0.78}W_{0.22}O_3$	$Mo_{0.81}W_{0.19}O_{2.96}$	$Mo_{0.54}W_{0.46}O_3$	$Mo_{0.51}W_{0.49}O_3$	$Mo_{0.24}W_{0.76}O_3$	$Mo_{0.16}W_{0.84}O_3$

The JCPDS card numbers (#) of the structures and the global stoichiometry of the samples are also reported.

monoclinic β-MoO_3 form is observed; this behavior was also reported in literature [37]. The diffraction patterns of MoW05 and MoW08 indicate high percentages of two phases: (i) for MoW05 sample $Mo_{0.6}W_{0.4}O_3$ [25] and the mixed oxide with the structure of β-MoO_3 and W occupancy of 0.49(4); (ii) for MoW08 sample $Mo_{0.29}W_{0.71}O_3$ [25] and $Mo_{0.14(6)}W_{0.86(6)}O_3$ with the structure of γ-WO_3 [36]. Also for MoW05 oxide a very low amount of the $Mo_{0.29}W_{0.71}O_3$ phase is present. On the basis of these results it is possible to estimate the global stoichiometry of the three samples as reported in Table 1: the calculated values are in good agreement with the initial synthesis stoichiometry. The cations occupancy values suggest that W substitutes the Mo ions in MoO_3 more easily than Mo in WO_3 structure, in agreement with previous observations [13].

For MoW05 and MoW08 the reducing treatment mainly induces structural rearrangements leading to changes in the relative amounts of the phases already present in the oxidized specimens and, in some cases, in their stoichiometry (see Table 1 and Fig. 1A). For MoW05, also monoclinic WO_3 segregates in significant amount (see peaks indicated by * in Fig. 1A). On the other hand, XRD pattern of reduced MoW02 shows the appearance of peaks due to a crystalline phase different from those of the oxidized sample and related to the presence of monoclinic $Mo_{0.85}W_{0.15}O_{2.91}$ sub-stoichiometric phase (main peaks indicated by (◦) in Fig. 1A) [38]. All the other observed phases (see Table 1) are those already discussed for the oxidized specimen; the cell volumes slightly expand (0.2–1.9%), probably because of the oxygen loss in the reduced phases, that induces the formation of Mo^{5+} and W^{5+}, with higher ionic radii with respect to the +6 oxidation state. The sub-stoichiometric phase disappears and the cell volume reaches the value expected in the oxidized samples for subsequent treatment in oxygen at 673 K, demonstrating the reversibility of the effect induced by the reducing treatment at 673 K. These results enlighten only for MoW02 mixed oxide the capability of losing a significant amount of oxygen, not only from the surface but also from the bulk up to a reversible structural rearrangement by crystallographic shear processes.

It is worth noting that the most of the phases evidenced by XRD both for the oxidized and reduced samples show the presence of different types of cationic sites with various symmetry. In particular, β-MoO_3, γ-WO_3 and $Mo_{0.29}W_{0.71}O_3$ show two cationic sites M1 and M2 with two differently distorted octahedral coordinations. The sub-stoichiometric phase $Mo_{0.85}W_{0.15}O_{2.91}$, evidenced for reduced MoW02, shows six cationic sites in differently distorted octahedrons. α-MoO_3 and $Mo_{0.6}W_{0.4}O_3$ structures have only one type of cationic site.

Since MoW02 demonstrated a big capability to lose oxygen, its preparation was also tried in a different way: the precursor (the hydrated oxide) was treated at 723 K in N_2 (and not O_2) flow. A black powder was obtained. In Fig. 1C the pattern of the N_2 treated sample (MoW02-N2) is compared with that prepared in O_2 (MoW02-re-ox). The former shows a very low degree of crystallinity, and the XRD pattern was refined with the Rietveld method on the basis of the structural parameters pertinent to the sub-stoichiometric Mo_9O_{25} phase (#81-1263 JCPDS) [39]. In the refinement, Mo/W ratio was maintained equal to 4; only the lattice parameters, the cation thermal factors and the profile parameters were varied. The agreement of the calculated profile with the experimental one is quite good. After annealing in oxygen at 723 K, the powder previously treated in N_2 shows the same color and the same diffraction peaks of the mixed oxide directly prepared by calcination in oxygen flow. The ability of this sample to take oxygen and to pass from an almost amorphous state to a perfect crystalline one, simply by contact with O_2 at 723 K, is surprising.

3.2. Spectroscopic characterization

3.2.1. Activated samples

In Fig. 2 UV–vis–NIR (A), FT-IR (B) and EPR (C) spectra of MoO_3 (a), WO_3 (b), MoW02 (c), MoW05 (d) and MoW08 (e) after the activation (evacuation and oxidation in O_2 at 723 K) are reported. In the high wavenumber side of the UV–vis–NIR spectra the absorption edges related to the electronic transition from the valence band to the conduction band are observed. For all the samples the intensity linearization as an indirect transition gives good results [40]. The band gap values are about 23 400 cm^{-1} (~2.9 eV) for MoO_3 [11,41–43], 21 000 cm^{-1} (~2.6 eV) for WO_3 [44,45], 21 800 cm^{-1} (~2.7 eV) for MoW02, 21 000 cm^{-1} (~2.6 eV) for MoW05 and 18 500 cm^{-1} (~2.3 eV) for MoW08. Among the mixed oxides only MoW02 is substantially constituted by a single crystalline phase; for MoW05 and MoW08 the observed band gap can be considered an average of the values of the single Mo–W phases constituting the two samples. The band gap of the Mo–W samples decreases on increasing tungsten content, in agreement with the results of Hoppmann et al. [28] for mixed oxides with different Mo/W content.

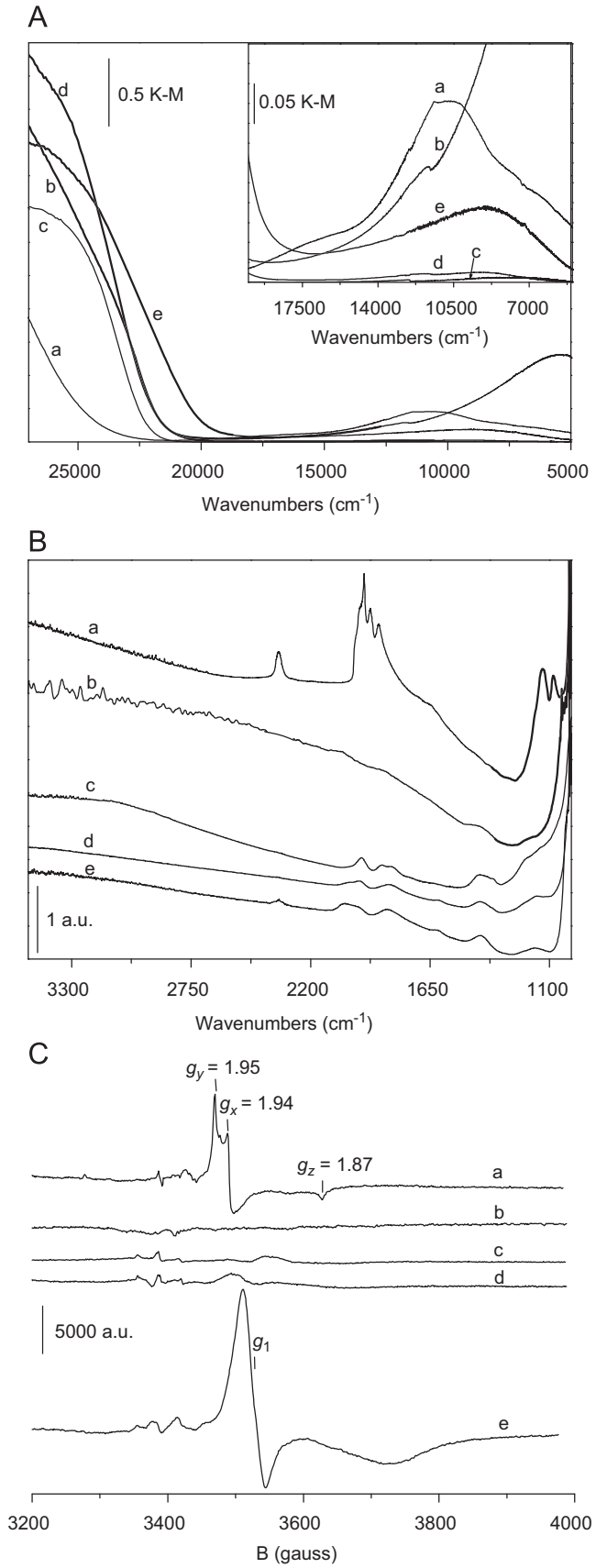

Fig. 2. UV–vis–NIR (section A, inset: magnification of the low wavenumber region), FT-IR (section B) and EPR (section C) spectra of MoO_3 (a), WO_3 (b), MoW02 (c), MoW05 (d) and MoW08 (e) after the activation at 723 K.

At energy below the fundamental absorptions (inset of Fig. 2A), broad bands are present for all the samples (very weak for MoW02 and MoW05). These absorption bands are related to the presence of electrons trapped in defect sites deriving from oxygen deficiency and they can be assigned to polaronic transitions ($M^{5+} \rightarrow M^{6+}$ metal to metal charge transfers) [24,28]. However, they can be also attributed to M^{5+} d–d transitions and to M^{5+}–O^{2-} ligand to metal charge transfers [11,12]. The presence of these bands evidences an intrinsic defectivity that resists to oxidation at 723 K, mainly for the two pure oxides and MoW08 mixed oxide.

In the MIR region (Fig. 2B) all the samples present the cut off at $\overline{\nu} < 1000-1100\,cm^{-1}$ due to the lattice vibrational modes. On the high wavenumber side of the spectra all the samples show the characteristic shape due to the radiation scattering (an apparent monotonic absorption that increases in intensity on increasing radiation energy). MoO_3 spectrum shows both in the range 1000–1250 and 1800–2000 cm^{-1} bands assignable to combinations of lattice vibrational modes [46]. The band at 2350 cm^{-1} can be attributed to CO_2 encapsulated in the oxide matrix and weakly interacting with the material. Also for the mixed oxides the weak bands in the region 1300–2000 cm^{-1} are reasonably assignable to combinations of lattice vibrational modes.

In Fig. 2C EPR spectra of all activated samples are reported. MoO_3 shows intense signal (Fig. 2C, curve a) with $g_1 = 1.94$, $g_2 = 1.95$ and $g_3 = 1.87$ characteristic of Mo^{5+} ions in 6-fold coordination with rhombic distortion [47]. No EPR signals are detected for WO_3 (Fig. 2C, curve b), so that the absorption of the sample in the Vis–NIR region must be attributed to species EPR-silent in dark condition, as better revealed with reduction and re-oxidation cycles at increasing temperature. The mixed oxides MoW02 (Fig. 2C, curve c), MoW05 (Fig. 2C, curve d) and MoW08 (Fig. 2C, curve e) have EPR signals related only to Mo^{5+} species, very weak for MoW02 and MoW05 and more intense for MoW08, paralleling the absorption intensities in the Vis–NIR region (Fig. 2A).

3.2.2. *Samples reduced in vacuum and re-oxidized*

In the following the evolution of the spectra on increasing the outgassing temperature and the reversibility in oxygen at increasing temperature will be discussed. For sake of clarity the point defects and the related spectroscopic features formed upon the reduction of each sample are reported in Table 2.

MoO_3: UV–Vis–NIR, difference FT-IR and EPR spectra of MoO_3 after treatment in vacuum at increasing temperature are reported in Fig. 3. In the Vis–NIR region (Fig. 3A) the broad absorptions already present after the initial activation (curve 1) increase in intensity on increasing the outgassing temperature. The phenomenon is reversible and the spectrum recovers the initial intensity after treatment in oxygen at 673 K. This behavior is thus related to the oxygen loss (producing defect sites with excess electrons) and to its reincorporation. In the envelope of the broad absorptions it is possible to distinguish at least a maximum centered at 10 800 cm^{-1} and two shoulders approximately at 7500 and 17 000 cm^{-1}. Salje and Hoppmann [28] assigned to a $Mo^{5+} \rightarrow Mo^{6+}$ intervalence charge transfer (polaronic) transition a broad band at 1.32 eV (~10 700 cm^{-1}) in the spectrum of a sub-stoichiometric $MoO_{2.99}$ oxide. More recently, Dieterle et al. [12] reported for orthorhombic MoO_3 with different reduction levels absorptions at about 7600 and 15 500 cm^{-1} assigned to d–d transition and $Mo^{5+} \rightarrow Mo^{6+}$ polaronic transition, respectively. On this basis, we assigned the absorption at about 10 800 and 17 000 cm^{-1} to polaronic transitions and that at 7500 cm^{-1} to d–d transition.

In the MIR region (Fig. 3B), along with the tail of the absorptions just described, a broad band with a maximum at

Table 2
Main point defects and their spectroscopic features for the reduced samples.

Samples	Point defects	Spectroscopic features		
		UV–vis–NIR (cm^{-1})	FT-IR (cm^{-1})	EPR
MoO_3	Mo^{5+} (bulk)	10800, 17000 ($Mo^{5+} \rightarrow Mo^{6+}$) 7500 ($Mo^{5+}$ d–d)		$g_1=1.94$ $g_2=1.95$ $g_3=1.87$ $g=1.98$
	V_O^+ (bulk and surface)		2350 ($V_O^+ \rightarrow$ C.B.)	$g=2.00$
WO_3	W^{5+}–W^{5+} (bulk) V_O^+ (surface and sub-surface)	5500 ($W^{5+} \rightarrow W^{6+}$)	 2300 ($V_O^+ \rightarrow$ C.B.)	Silent in dark conditions $g=2.00$
MoW02	Mo^{5+} (bulk) Mo^{5+} (bulk) near to W^{6+} V_O^+ (bulk)	5000–20 000 ($Mo^{5+} \rightarrow Mo^{6+}$; $Mo^{5+} \rightarrow W^{6+}$; Mo^{5+} d–d)	 3200 ($V_O^+ \rightarrow$ C.B.)	$g_1=1.94$ $g_2=1.95$ $g=1.90$ $g=2.00$
MoW05	Mo^{5+} (bulk and surface)	8400 ($Mo^{5+} \rightarrow W^{6+}$)		$g_1=1.93$ $g_2=1.94$ $g=1.90$
MoW08	Mo^{5+} (bulk)	9000 ($Mo^{5+} \rightarrow W^{6+}$)		$g=1.93$ $g=1.90$

about 2350 cm^{-1} is observable. Though never reported in the literature for MoO_3, electronic absorptions in this region are reported for semiconducting oxides like SnO_2 and ZnO [48–50]: they are assigned to electron transitions from shallow levels, mainly mono-ionized oxygen vacancies (V_O^+), to the conduction band. The assignment is supported by the fact that oxygen vacancies are the predominant point defects in these oxides and that the energies of ionization of the bulk V_O^+ in the single-crystals are known: 0.145 eV (1170 cm^{-1}) and 0.18 eV (1450 cm^{-1}) for SnO_2 and ZnO, respectively [51–53]. By analogy it is possible to tentatively assign the band at 2350 cm^{-1} in the spectra of MoO_3 to the photo-ionization of mono-ionized oxygen vacancies.

The shape of the MIR spectra in Fig. 3B is complicated by the presence of negative peaks: (i) in the region 1800–2000 cm^{-1} related to the combination of lattice vibrational modes; (ii) at 2350 cm^{-1} related to encapsulated CO_2 (Fig. 2B, curve a). We assigned the erosion of these peaks to a coupling process between electronic transitions and vibrational modes. The theory of Genzel and Martin [54] concerning optical properties of small particles of conducting and semiconducting materials gives an explanation of a similar phenomenon when plasmon absorptions are involved. When the concentration of the free carriers (in the specific case free electrons in the conduction band) is high enough to cause the plasmon frequency to overcome the phonon frequency a plasmon–phonon coupling process occurs leading to the disappearance of any band of a purely vibrational nature. It is experience of our group the observation of a coupling process between electronic absorption related to photo-ionization of mono-ionized oxygen vacancies and the vibrations of surface species on semiconducting oxides such as SnO_2 and ZnO [55].

EPR spectra (Fig. 3C) provide further information. Firstly, it can be observed that the intensity of the signals previously assigned to Mo^{5+} ions increases on increasing temperature, while, simultaneously, the spectrum becomes progressively broader. Spectra 3 and 4 are, most likely, an envelope of similar signals whose individual features are not easily distinguished. EPR signals of Mo^{5+} species in different coordination states and symmetries, resonating in the range of magnetic field of spectra in Fig. 3C, are reported in literature. For example, a signal with $g_1=1.959$, $g_2=1.953$ and $g_3=1.867$ was attributed to Mo^{5+} in 5-fold coordination with a distorted quadratic-pyramidal environment [56–58]. Another with g-values at $g_\perp=1.935$ and $g_\parallel=1.901$ was assigned to a 6-fold coordinated Mo^{5+} centers in an axially distorted MoO_6 octahedron. Furthermore, the component visible at $g=1.98$ could be due to a Mo^{5+} species, that, unlike those described above, has lost the molybdenyl oxygen. In this case, a Mo^{5+} species surrounded by a distorted square pyramidal environment of oxygen ions was associated to a signal with $g_1=1.891$, $g_2=1.978$ and $g_3=1.984$ [59]. Summarizing, several variously coordinated Mo^{5+} species, could, in principle, contribute to the spectra in Fig. 3C, whose line-width progressively increases with increasing the solid defectivity.

The EPR spectra are thus in agreement with the results obtained by UV–vis–NIR spectroscopy and in addition shows a variety of coordinations and symmetries for reduced Mo^{5+} species. Both the absorptions in the vis–NIR region and the EPR signals related to Mo^{5+} species formed after treatment in vacuum at 673 K are quite resistant to subsequent treatment in oxygen at increasing temperature: after oxidation at 573 K the situation is almost the same reached after outgassing at 673 K. It is necessary to oxidize the sample at 673 K to recover the situation of spectrum 1 in Fig. 3A and C. This suggests that Mo^{5+} species are formed preferentially in the bulk of the material.

Furthermore, in Fig. 3C a sharp isotropic signal at $g=2.00$ (thus close to the free electron $g_e=2.0023$) is observed. This signal was already reported in literature for MoO_3: Mestl et al. [46,56] attributed it to F centers, i.e. electrons trapped in oxygen vacancies (or V_O^+). This result is in agreement with the increase of the broad absorption at 2350 cm^{-1} (Fig. 3B) assigned to the photo-ionization of mono-ionized oxygen vacancies. The intensity of the EPR signal at $g=2.00$ is maximum after outgassing at 573 K and decreases for outgassing at 673 K: a reasonable explication is that the amount of electrons trapped in oxygen vacancies is high enough to make them to interact, eliminating part of the signal. Subsequent interaction with oxygen at increasing temperature gradually restores the initial situation for EPR signal and for the absorption in the MIR region: the gradual erosion suggests a regular distribution of the vacancies both on the surface and in the bulk of the material.

WO_3: The spectroscopic results concerning WO_3 are reported in Fig. 4. UV–vis–NIR spectra (Fig. 4A) show a progressive increase, with increasing the reduction degree of the broad band with maximum at about 5500 cm^{-1} (already observed for the oxidized sample, Fig. 2A) showing a very weak shoulder on its high wavenumber wing. The initial situation is recovered by treatment in oxygen at high temperature, indicating that, once again, the

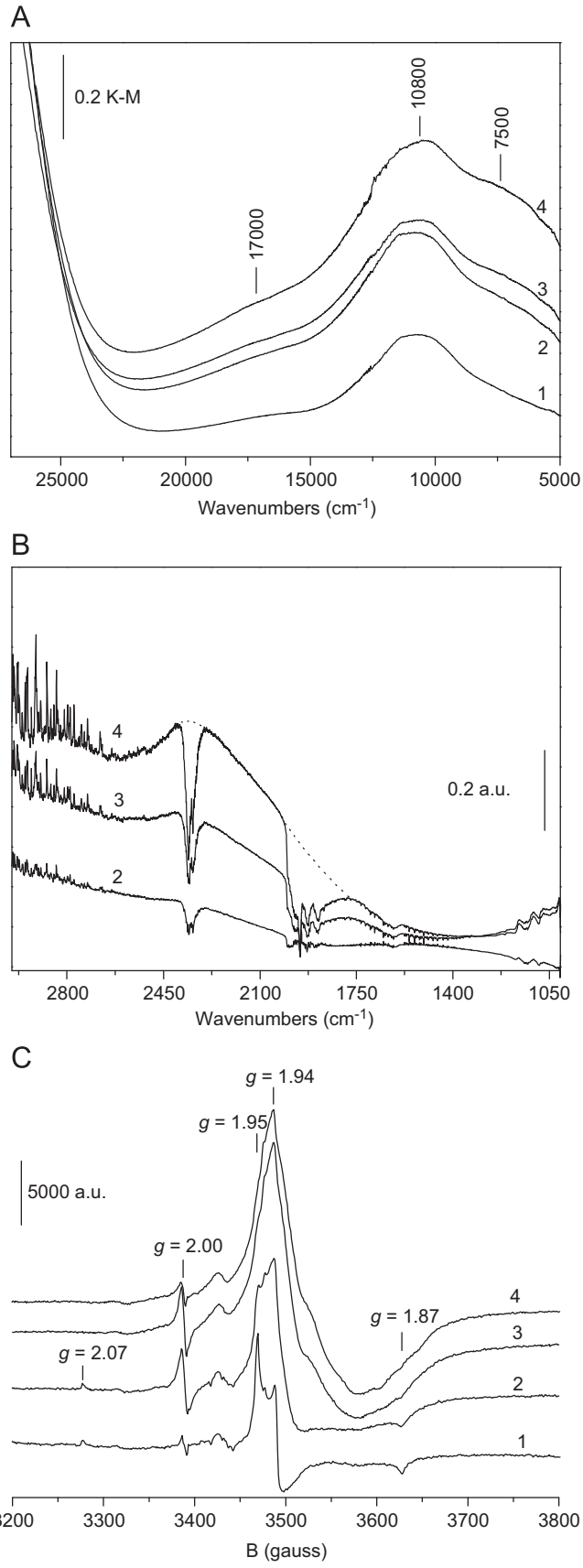

Fig. 3. UV–vis–NIR (section A), difference FT-IR (section B) and EPR (section C) spectra of MoO_3 after the activation at 723 K (1) and subsequent outgassing at 473 K (2), 573 K (3) and 673 K (4). Spectra are recorded at RT in the UV–vis–NIR and MIR regions, at 77 K for EPR.

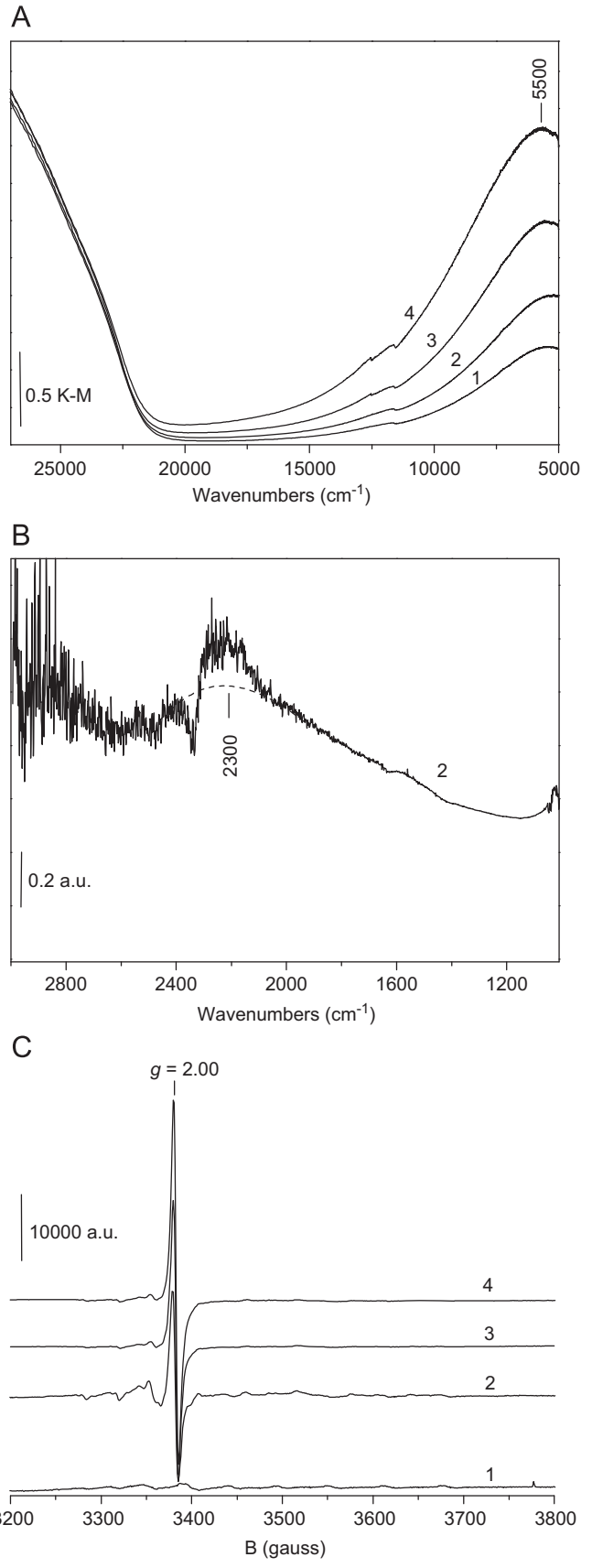

Fig. 4. UV–vis–NIR (section A), difference FT-IR (section B) and EPR (section C) spectra of WO_3 after the activation at 723 K (1) and subsequent outgassing at 473 K (2), 573 K (3) and 673 K (4). Spectra are recorded at RT in the UV–vis–NIR and MIR regions, at 77 K for EPR.

reversible phenomenon is due to the loss of oxygen that produces defect sites with trapped electrons. As seen for MoO_3, we can relate the band to the presence of W^{5+} species. Actually, a band at 0.7 eV ($\sim$5600 cm^{-1}) and one at 0.82 eV in the spectrum of sub-stoichiometric $WO_{2.99}$ and $WO_{2.72}$ oxide, respectively, has been assigned to $W^{5+} \rightarrow W^{6+}$ polaronic transition by Salje and Schirmer [9,28,60]. The absorption formed after treatment in vacuum at 673 K is quite resistant to subsequent treatment in oxygen at increasing temperature: only oxidation at 573 K causes an appreciable decrease of the band, but it is necessary to oxidize the sample at 673 K to recover the situation of spectrum 1. This indicates that W^{5+} species are formed preferentially in the bulk of the material.

Fig. 4B illustrates the spectrum in the MIR region obtained after outgassing at 473 K: it is very noisy and its shape is unclear. Reasonably, it is constituted by the overlapping of two contributions: the tail of the band observed in the vis–NIR region and a band having a maximum at about 2300 cm^{-1} and assignable to the photo-ionization of mono-ionized oxygen vacancies. At higher temperatures the sample becomes completely absorbent towards radiation.

The EPR spectra of progressively reduced WO_3 (Fig. 4C) are dominated by a narrow signal at g=2.00, very closed to the free electron value. This signal is very intense and, to our knowledge, in literature this kind of signal was never reported for WO_3. It is reasonably due to electrons trapped in oxygen vacancies and this result confirms what observed in the MIR region. The sharp signal at g=2.00 is completely eliminated by treatment in oxygen at 473 K, but already at room temperature and at 373 K the erosion of the signal is consistent: this result suggests that oxygen vacancies with trapped electron are preferentially on the surface and sub-surface layers.

On the contrary, no EPR signals related to W^{5+} species are observed. W^{5+} signals at g_x=1.50–1.39, g_y=1.66–1.70 and g_z=1.53–1.54 are expected at high field having g values in the range 1.70–1.40 [60–63]. However, the spin lattice relaxation time for 5*d* and 4*d* ions is relatively short compared to 3*d* ions [64], so that observation of their EPR signals is limited at very low temperature. We have thus recorded EPR spectra at 4 K, but even at this temperature no signals related to W^{5+} species appeared. Nevertheless, it is well known the possibility for W to form bipolarons (W^{5+}–W^{5+}) [9,22,28,29,60]: in this case the electrons in the ground state are trapped not singly but in pairs at neighboring W^{5+} sites and may be associated with some metal–metal bonding occurring between edge-sharing WO_6 octahedra in the reduced compound. Bipolarons are diamagnetic and, for this reason, EPR-silent; it possible to observe W^{5+} EPR signals only under irradiation with light, as experimented by Schirmer et al. [9,60]. So, on one hand, we can conclude that in our sample, under dark conditions, all W^{5+} species are present as bipolarons and that EPR reveals only the presence of electrons in mono-ionized oxygen vacancies. On the other hand, the presence of unpaired W^{5+} is revealed by the absorption at about 5500 cm^{-1} in the vis–NIR spectra, that we assign to the polaronic transition as reported in literature [9]. In fact, the bipolaronic transition should fall at higher wave-numbers, in the range 1.1–1.3 eV (9000–10 500 cm^{-1}) [29,60]. The results coming from the two spectroscopies (EPR and UV–vis–NIR), apparently non-consistent, can be attributed to the fact that the W^{5+} pairs are very sensitive to dissociation by the light and are effectively broken by the measuring light, as already reported [9]. Actually, the weak shoulder on the high wave-number wing of the absorption at 5500 cm^{-1} can be assigned to the bipolaronic transition.

MoW02: The MoW02 mixed oxide shows spectra in the vis–NIR region (Fig. 5A) characterized by a very broad absorption peaked at about 9000 cm^{-1} with a shoulder at about 16 000 cm^{-1}.

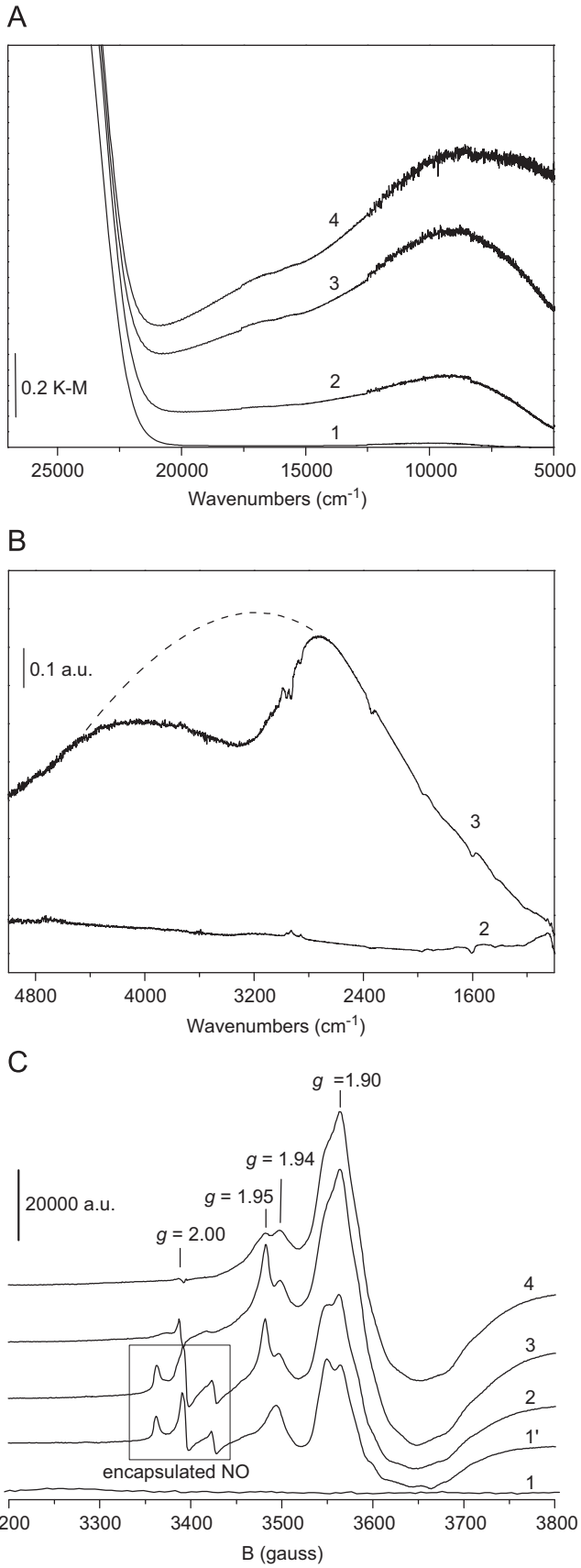

Fig. 5. UV–vis–NIR (section A), difference FT-IR (section B) and EPR (section C) spectra of MoW02 after the activation at 723 K (1) and subsequent outgassing at 473 K (2), 573 K (3) and 673 K (4). Spectra are recorded at RT in the UV–vis–NIR and MIR regions, at 77 K for EPR. In section C spectrum after outgassing at 373 K (1′) is also reported.

Following the assignment made for the molybdenum and tungsten oxides, these bands can be related to the presence of Mo^{5+} and W^{5+} species. The erosion in oxygen of the vis–NIR bands is consistent above 573 K: this is an indication that M^{5+} sites are preferentially in the bulk of the mixed oxide, as already observed for MoO_3 and WO_3. After oxidation at 673 K the spectrum recovers the situation of curve 1 in Fig. 5A.

In the MIR region (Fig. 5B) broad bands increase. The shape of the spectrum after outgassing at 573 K (spectrum 3; at 673 K the sample is completely absorbent) is somewhat strange. The minimum around 3300 cm^{-1} correspond to a negative trend related to hydroxyl vibrational modes and induces to think about the coupling process between electronic and vibrational absorptions, already observed for MoO_3. The broad electronic absorption thus qualitatively reconstructed (dotted line in Fig. 5B) with a maximum at about 3200 cm^{-1} is assignable to the photoionization of mono-ionized oxygen vacancies.

As for the subsequent treatment in oxygen, up to 573 K, the shape of the MIR spectra does not change. It is necessary to oxidize at 673 K to return to the initial situation: unlike molybdenum and tungsten oxides, the oxygen vacancies with trapped electrons are preferentially in the bulk.

The interpretation of the EPR spectra of MoW02 (Fig. 5C) is rather complex. On the activated sample (curve 1) very weak signals are present but, unlike MoO_3 and WO_3, already the outgassing at 373 K (curve 1′) causes the appearance of quite intense spectrum, dominated by signals due to reduced Mo^{5+} species. A minor quantitative role is shown by a triplet centered around g=2.00 and due to molecular NO impurities formed during the synthesis [65]. The NO species is eliminated rising the temperature treatment so allowing the observation of a very weak signal assignable to electrons trapped in oxygen vacancies (line 3). The Mo^{5+} species contributing to the spectrum are at least two. The former is the same observed for reduced MoO_3 with g_1 and g_2 at 1.94 and 1.95. The trace of this species is partially buried into the intense and broad signal having $g_\perp$ at about 1.90 and unresolved parallel features. This signal, not observed in the case of MoO_3, has to be ascribed to Mo^{5+} centers formed in the reduced W-containing mixed Mo–W–O phases. Small changes in the coordinative environment of Mo^{5+}, due to the presence of tungsten ions, are sufficient to explain the g-shift of this new signal. Actually, structural characterization has evidenced that for pure MoO_3 both oxidized and reduced samples show the presence of the α-MoO_3 phase with only one kind of cationic site, but the introduction of tungsten induces, both on oxidized and reduced samples, the formation of phases with at least two kinds of cationic sites into differently distorted octahedrons. The high line-width of the second signal at higher field is likely due to the dipolar broadening and structural heterogeneity. The centers are therefore not isolated but magnetically interacting.

As observed for WO_3, for MoW02 no signals are present at g-values characteristic of W^{5+}, but differently from WO_3, for MoW02 we can exclude or consider extremely improbable the presence of W^{5+} pairs, since tungsten is the minority component and ordered mixed phases with molybdenum are formed. The results shown by EPR are, therefore, rather consistent with the fact that the six-valent state of tungsten is more stable than the six-valent state of molybdenum. Actually, studies performed by X-ray photoelectron spectroscopy on reduced $Mo_{0.2}W_{0.8}O_{2.94}$ crystals [27] showed that ca. 20% Mo, but only 1.3% W appears in the five valent state. The preferential reduction of Mo is explained by its slightly lower trapping energy with respect to W.

Therefore, coming back to the assignment of the absorptions in UV–vis–NIR spectra, the observed absorptions are assigned to electronic transitions starting from Mo^{5+} species, in particular, to $Mo^{5+} \rightarrow Mo^{6+}$ and $Mo^{5+} \rightarrow W^{6+}$ transitions. However, in our opinion a contribution to the absorption due to Mo^{5+} d–d transition cannot be excluded.

All the EPR signals related to Mo^{5+} species are markedly reduced in oxygen at 573 K and are eliminated at 673 K only, according with what observed by UV–vis–NIR spectra. They are bulk defects as indicated not only by spectroscopic techniques, but also by XRD results that put into evidence the presence of a stable $Mo_{0.85}W_{0.15}O_{2.91}$ in the reduced sample (see Table 1).

MoW05 and MoW08: The intensities of the bands in the Vis–NIR region and of the EPR signals increase gradually on increasing temperature for both samples (spectra not reported), as observed for the other specimens. For sake of brevity, only the UV–vis–NIR (Fig. 6A) and the EPR spectra (Fig. 6B) of MoW05 (curves a) and MoW08 (curves b) after treatment at 673 K are reported. Despite the different phases formed (Table 1) the spectra of the two materials look quite similar. In the vis–NIR region (Fig. 6A) MoW05 and MoW08 show absorbance band with maximum at 8400 and 9000 cm^{-1}, respectively, related to the presence of M^{5+}

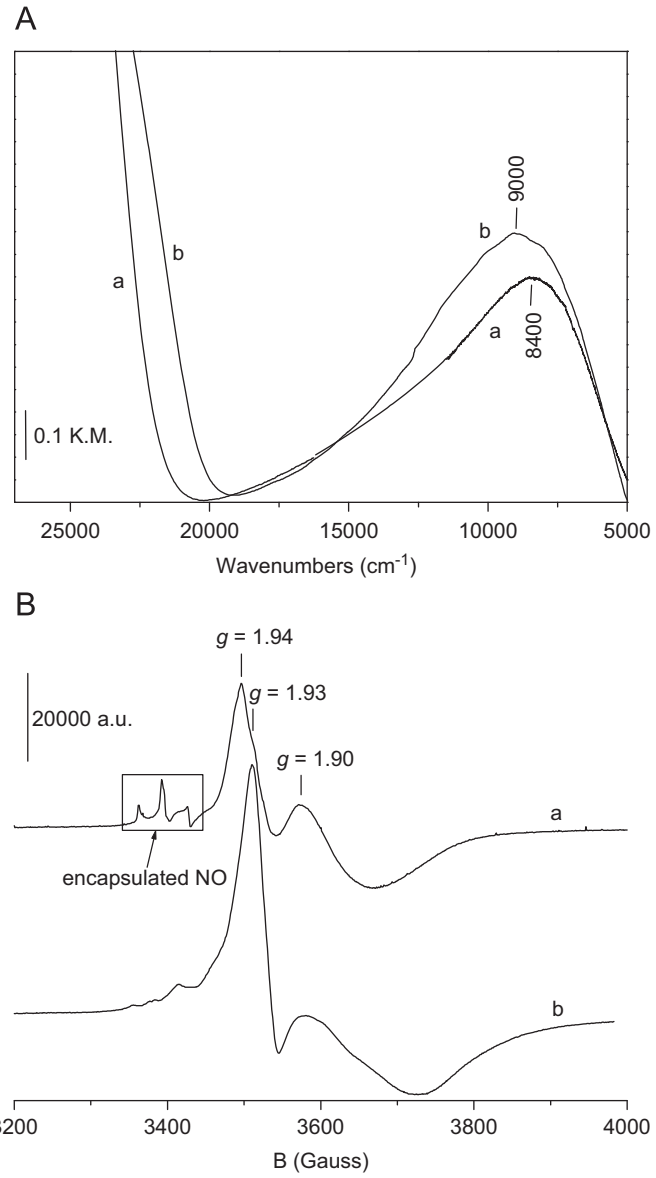

Fig. 6. UV–vis–NIR (section A) and EPR (section B) spectra of MoW05 (a) and MoW08 (b) after treatment in vacuum at 673 K. UV–vis–NIR spectra are recorded at RT, EPR spectra at 77 K.

species. The EPR spectra (Fig. 6B) of both MoW05 and MoW08 are basically constituted by signals observed for MoW02, the most important difference being the high line-width of the Mo^{5+} signal at higher field. The signal of MoW08 recorded at 4 K (not reported) does not change and no signal at *g*-value typical of W^{5+} appears. The broad nature of the Mo^{5+} signal at high field is thus not due to the variation of T2 (spin–spin relaxation time) depending on the temperature. The phenomenon is similar to that observed on reduced rutile TiO_2 and is due to the presence of magnetically interacting reduced centers in a heterogeneous environment disordered by the effect of reduction. Moreover, we have to keep in mind that structural characterization revealed that also these mixed oxides, both oxidized and reduced, are constituted by phases with at least two kinds of cationic sites into differently distorted octahedrons.

MoW05 and MoW08, differently from MoW02, do not present absorptions in the MIR region (spectra not reported), but only show the tail of the absorptions present in the NIR region. Accordingly, in the EPR spectra (Fig. 6B) no signal at $g=2.00$ related to free or trapped electrons is observed. Thus, the presence of mono-ionized oxygen vacancies in the two samples can be ruled out.

As for the reversibility in oxygen, the behaviors of MoW05 and MoW08 are different. For MoW05 a fraction of EPR signals are eliminated already at RT (see Fig. 7, curve 2): on one hand a sensible decrease of the *g* signal at 1.93–1.94 after oxidation at RT occurs; on the other hand the intensity increase of the broad *g* signal at 1.90 (evidenced by the arrow in the figure), reasonably, is only apparent, owing to the modification of the overall trace of the species with *g* signal at 1.93–1.94. Thus, for MoW05 a consistent part of Mo^{5+} species is on the surface of the sample. The other fraction of Mo^{5+} signals is gradually eroded with increasing the temperature and assignable to bulk defect sites. The evolution in oxygen at increasing temperature of the broad band in the vis–NIR region confirms the presence of defect sites eliminated already at RT. For MoW08 both the band in the vis–NIR region and the signals in the EPR spectra are only slight eroded in oxygen at RT. At 573 K the 40% of their intensities is eroded. Only the oxidation at 673 K brings the situation to that of the pre-treated sample shown in Fig. 2C. Thus, we can conclude that for MoW08 M^{5+} species are mainly bulk defects.

The tungsten concentration for these two mixed samples could allow the formation of W^{5+} pairs, and this should be the reason for the absence of EPR signal at *g*-value typical of W^{5+}. If so, as observed for WO_3, the W^{5+} pairs, very sensitive to dissociation by the light, should be effectively broken by the measuring light during the run of the optical spectra. Therefore, in the vis–NIR spectra of MoW05 and MoW08 samples outgassed at increasing temperature, the component at about 5500 cm^{-1}, assigned to W^{5+} polarons, should appear. This is not the case. Moreover, as discussed before, the erosion of the absorption bands in the vis–NIR region, on one hand, and the signals in the EPR spectra, on the other hand, proceed in the same way with the temperature. Thus, it is reasonable to admit a correlation between the EPR and the vis–NIR spectroscopic features both assignable to the same Mo^{5+} species. We can logically conclude that both W polarons and bipolarons are absent and, as observed for MoW02 sample, the electrons released during the reduction treatments are trapped by molybdenum. For MoW05 and MoW08 UV–vis spectra are less complex than those observed for MoW02, for which we hypothesized the presence of both $Mo^{5+} \rightarrow Mo^{6+}$ and $Mo^{5+} \rightarrow W^{6+}$ transitions; taking into account the high W concentration for these mixed oxides the UV–vis absorption can be assigned mainly to the $Mo^{5+} \rightarrow W^{6+}$ transition [28].

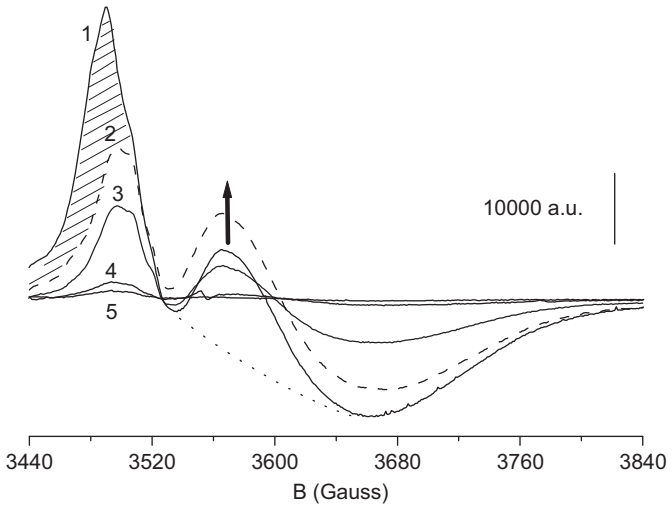

Fig. 7. EPR spectra of MoW05 sample after treatment in vacuum at 673 K (1) and after treatment in O_2 at RT (2), 473 K (3), 573 K (4) and 673 K (5).

4. Conclusions

The combined use of X-ray diffraction, diffuse reflectance UV–vis–NIR, absorbance FT-IR and EPR spectroscopies was adopted to determine the property of MoO_3, WO_3 and Mo–W mixed oxides to lose oxygen and to form defect sites with trapped electrons, such as polarons (M^{5+}) and mono-ionized oxygen vacancies (V_O^+). XRD analysis of the oxidized samples show that the Mo–W mixed oxides are always constituted by at least two distinct phases with different abundances and whose stoichiometry is evaluated by the Rietveld method. Only the sample with the highest Mo content (Mo/W molar ratio=4) shows a predominant mixed phase. The composition recalculated on the basis of phase abundances and stoichiometry well agrees with that of the synthesis. After reducing treatments in vacuum at increasing temperature all molybdenum containing samples show the formation of Mo^{5+} centers in a variety of coordinations and symmetries; MoO_3 and MoW02 show the presence of mono-ionized oxygen vacancies. A significant abundance of electrons trapped at oxygen vacancies is shown by WO_3 along with the presence of W^{5+} species paired to form EPR-silent bipolarons. UV–vis–NIR spectroscopy combined with EPR one also shows the absence of W^{5+} species (either isolated or paired in bipolarons) in all the mixed oxides. Electrons related to the loss of oxygen are preferentially trapped by molybdenum cations, being Mo^{5+} ion energetically favored with respect to W^{5+}.

XRD technique reveals that the oxygen loss in vacuum at 673 K is related to relevant crystallographic shear process only for MoW02 mixed oxide: this material exhibits the best capability to lose oxygen from the bulk in reducing conditions, until showing the formation of additional diffraction peaks of a phase different from those of the oxidized sample. Moreover, the structural changes induced by the oxygen loss in MoW02 are totally reversible for treatment in oxygen at 673 K.

Reducing and oxidizing cycles allow to determine the surface or bulk nature of the defects. In particular, in MoO_3 mono-ionized oxygen vacancies are both on the surface and in the bulk and Mo^{5+} polarons preferentially in the bulk of the material; in WO_3 mono-ionized oxygen vacancies are preferentially on the surface or sub-surface layers and W^{5+}–W^{5+} bipolarons preferentially in the bulk; for MoW02 both mono-ionized oxygen vacancies and Mo^{5+} species are mainly in the bulk of the material, the same for the Mo^{5+} polarons in MoW08 mixed oxide. Moreover, MoW05 shows a consistent part of Mo^{5+} defect sites on the surface.

Acknowledgment

The authors thank the Regione Piemonte Council (Italy) for the financial support to a project entitled "Sintesi e caratterizzazione di materiali ossidici nano-strutturati" (Project no. CIP4).

References

[1] Y. Djaoued, P.V. Ashrit, S. Badilescu, R. Brüning, J. Sol–Gel Sci. Technol. 28 (2003) 235.
[2] I. Karakurt, J. Boneberg, P. Leiderer, Appl. Phys. A 83 (2006) 1.
[3] R. Solarska, B.D. Alexander, J. Augustynski, J. Solid State Electrochem. 8 (2004) 748.
[4] M. Dieterle, G. Mestl, J. Jäger, Y. Uchida, H. Hibst, R. Schlögl, J. Mol. Catal. 174 (2001) 169.
[5] S.B. Abd Hamid, D. Othman, N. Abdullah, O. Timpe, S. Knobl, D. Niemeyer, J. Wagner, D. Su, R. Schlögl, Top. Catal. 24 (2003) 87.
[6] S.Y. Chai, Y.J. Kim, W.I. Lee, J. Electroceramics 17 (2006) 909.
[7] R. Jin, X. Xia, W. Dai, J. Deng, H. Li, Catal. Lett. 62 (1999) 201.
[8] R. Gehlig, E. Salje, Philos. Mag. 47 (1983) 229.
[9] O.F. Schirmer, E. Salje, J. Phys. C. Solid State Phys. 13 (1980) L1067.
[10] P.A. Cox, Transition Metal Oxides, Clarendon Press, Oxford, 1995.
[11] G. Mestl, N.F.D. Verbruggen, H. Knözinger, Langmuir 11 (1995) 3035.
[12] M. Dieterle, G. Weinberg, G. Mestl, Phys. Chem. Chem. Phys. 4 (2002) 812.
[13] T. Ekström, E. Salje, R.J.D. Tilley, J. Solid State Chem. 40 (1981) 75.
[14] D. Wang, D. Su, R. Schlögl, Crys. Res. Technol. 2 (2003) 153.
[15] L. Lozzi, L. Ottaviano, M. Passacantando, S. Santucci, C. Cantalini, Thin Solid Films 391 (2001) 224.
[16] C.S. Rout, K. Ganesh, A. Govindaroj, C.N.R. Rao, Appl. Phys. A 85 (2006) 241.
[17] M. Ferroni, V. Guidi, G. Martinelli, P. Nelli, M. Sacerdoti, G. Sberveglieri, Thin Solid Films 307 (1997) 148.
[18] M. Ferroni, V. Guidi, G. Martinelli, M. Sacerdoti, P. Nelli, G. Sberveglieri, Sens. Actuators B, Chem. 48 (1998) 285.
[19] K. Galatsis, Y.X. Li, W. Wlodarsky, K. Kalantar-zadeh, Sens. Actuators B, Chem 77 (2001) 478.
[20] K. Galatsis, Y.X. Li, W. Wlodarsky, E. Comini, G. Sberveglieri, C. Cantalini, S. Santucci, M. Passacantando, Sens. Actuators B, Chem. 83 (2002) 276.
[21] K. Galatsis, Y.X. Li, W. Wlodarsky, C. Cantalini, M. Passacantando, S. Santucci, J. Sol–Gel Sci. Technol. 26 (2003) 1097.
[22] O. Merdrignac-Conanec, P.T. Moseley, J. Mater. Chem. 12 (2002) 1779.
[23] D. Gloeikler, F. Jeannot, C. Gleitzer, J. Less-Common Met. 36 (1974) 41.
[24] B.W. Faughnan, R.S. Crandall, Appl. Phys. Lett. 31 (1977) 834.
[25] E. Salje, R. Gehlig, K. Viswanathan, J. Solid State Chem. 25 (1978) 239.
[26] G. Hoppmann, E. Salje, Opt. Commun. 30 (1979) 199.
[27] E. Salje, A.F. Carley, M.W. Roberts, J. Solid State Chem. 29 (1979) 237.
[28] E. Salje, G. Hoppmann, Philos. Mag. B 43 (1981) 105.
[29] Y. Hiruta, M. Kitao, S. Yamada, Japan. J. Appl. Phys. 23 (1984) 1624.
[30] H. Gruber, E. Krautz, H.P. Fritzer, K. Gatterer, A. Popitsch, Phys. Status Solidi 98 (1986) 297.
[31] H. Gruber, E. Krautz, H.P. Fritzer, K. Gatterer, A. Popitsch, Solid State Commun. 58 (1986) 133.
[32] S. Morandi, G. Ghiotti, A. Chiorino, E. Comini, Thin Solid Films 490 (2005) 74.
[33] S. Morandi, G. Ghiotti, A. Chiorino, B. Bonelli, E. Comini, G. Sberveglieri, Sens. Actuators B, Chem. 111–112 (2005) 28.
[34] Bruker AXS, TOPAS V3.0: general profile and structural analysis software for powder diffraction data. User Manual Bruker AXS, Karlsruhe, Germany, 2005.
[35] J.B. Parise, E.M. McCarron III, R. Von Dreele, J.A. Goldstone, J. Solid State Chem. 93 (1991) 193.
[36] P.M. Woodward, A.W. Sleight, T. Vogt, J. Phys. Chem. Solids 56 (1995) 1305.
[37] S.-H. Baeck, T.F. Jaramillo, D.H. Jeong, E.W. McFarland, Chem. Commun. 4 (2004) 390.
[38] B. Blomberg, L. Kihlborg, A. Magneli, Ark. Kemi. 6 (1953) 133.
[39] F. Portemer, M. Sundberg, L. Kihlborg, M. Figlarz, J. Solid State Chem. 103 (1993) 403.
[40] J.I. Pankove, Optical Processes in Semiconductors, Dover Publications, New York, 1975.
[41] S.K. Deb, J.A. Chopoorian, J. Appl. Phys. 37 (1966) 4818.
[42] M.R. Tubbs, Phys. Status Solidi A 21 (1974) 253.
[43] R. Erre, M.H. Legay, J. Fripiat, Surf. Sci. 127 (1983) 69.
[44] F.P. Koffyberg, K. Dwight, A. Wold, Solid State Commun. 30 (1979) 422.
[45] R. Chatten, A.V. Chadwick, A. Rougier, P.J.D. Lindan, J. Phys. Chem. B 109 (2005) 3146.
[46] G. Mestl, T.K.K. Srinivasan, H. Knözinger, Langmuir 11 (1995) 3795.
[47] V.A. Ioffe, I.B. Patrina, E.V. Zelenetskaya, V.P. Mikheeva, Phys. Status Solidi 35 (1969) 535.
[48] G. Ghiotti, A. Chiorino, F. Boccuzzi, Surf. Sci. 287/288 (1993) 228.
[49] S. Lenaerts, J. Roggen, G. Maes, Spectrochim. Acta 51A (1995) 883.
[50] Z.M. Jarzebski, J.P. Marton, J. Electrochem. Soc. 123 (1976) 299C.
[51] Z.M. Jarzebski, J.P. Marton, J. Electrochem. Soc. 123 (1976) 333C.
[52] W. Gopel, U. Lampe, Phys. Rev. B 22 (1980) 6447.
[53] A. Hausmann, B. Schallenberger, Z. Phys. B 31 (1978) 269.
[54] L. Genzel, T.P. Martin, Surf. Sci. 34 (1973) 33.
[55] G. Ghiotti, A. Chiorino, F. Prinetto, Sens. Actuators B, Chem 24–25 (1995) 564.
[56] G. Mestl, N.F.D. Verbruggen, E. Bosh, H. Knözinger, Langmuir 12 (1996) 2961.
[57] E. Serwicka, J. Solid State Chem. 51 (1984) 300.
[58] K. Dyrek, M. Łabanowska, J. Chem. Soc., Faraday Trans. 87 (1991) 10003.
[59] M. Łabanowska, Phys. Chem. Chem. Phys. 1 (1999) 5385.
[60] O.F. Schirmer, E. Salje, Solid State Commun. 33 (1980) 333.
[61] R.R. Rakhimov, D.E. Jones, H.L. Rocha, A.I. Prokofév, A.I. Aleksandrov, J. Phys. Chem. 104 (2000) 10973.
[62] A. Punnoose, M.S. Seehra, Catal. Lett. 78 (2002) 157.
[63] M. Occhiuzzi, D. Cordischi, D. Gazzoli, M. Valigi, P.C. Heydorn, Appl. Catal. A. Gen. 269 (2004) 169.
[64] J.E. Wertz, J.R. Bolton, Electron Spin Resonance, McGraw-Hill, New York, 1972.
[65] S. Livraghi, A. Votta, M.C. Paganini, E. Giamello, Chem. Commun. (2005) 498.